

Chapter 2

FABRICATION PROCEDURE AND TESTING SETUP

2.1 Introduction

In this chapter, the fabrication procedures and the testing setups for the sub-micrometer lasers, the submicron disk laser and the photonic crystal laser are detailed. The fabrication and testing setups for the dye lasers are described in the corresponding chapters later on.

2.2 Wafer design and epitaxy growth

Our group has been working on the III-V epitaxy light emitting materials which could be grown by metalorganic vapour phase epitaxy (MOCVD), liquid phase epitaxy (LPE), and molecular beam epitaxy (MBE). Epitaxy describes an ordered crystalline growth on a monocrystalline substrate. Different from other thin-film deposition methods, such as thermal evaporation or ion sputter deposition which deposit polycrystalline or amorphous films even on single-crystal substrates, in epitaxy growth the deposited film takes on a lattice structure and orientation identical to those of the substrate. In other words, the substrate acts as a seed crystal. Previously, in our group, we mainly focused on the InGaAsP quantum well material system (Table 2.1) and InAs quantum dots within the InGaAs material (Table 2.2). Both of them emit light in the near infrared spectrum for the application of telecommunication. In this thesis, we will focus on the visible emission materials InGaP/InGaAlP quantum well material system (Table 2.3).

Materials	Function	comments	doping [1/cm ³]	thickness(nm)
p-InP	cap		1.00E+17	50
p-InGaAsP	carrier confinement		1.00E+17	97
i-InGaAsP	carrier confinement		undoped	20
i-InGaAsP	QW	.85%compressive strain	undoped	9
i-InGaAsP	barrier		undoped	20
i-InGaAsP	QW	.85%compressive strain	undoped	9
i-InGaAsP	barrier		undoped	20
i-InGaAsP	QW	.85%compressive strain	undoped	9
i-InGaAsP	barrier		undoped	20
i-InGaAsP	QW	.85%compressive strain	undoped	9
i-InGaAsP	carrier confinement		undoped	20
n-InGaAsP	carrier confinement		1.00E+17	97
n-InP	sacrificial layer		3e+18 ->1e+17	300
n-InP	sacrificial layer		3.00E+18	1200
n-InGaAs	etch stop		3.00E+18	20
n-InP	buffer		3.00E+18	400
n-InP	substrate			

Table 2.1 Layer structures of InGaAsP quantum well samples for infrared photonic crystal lasers

Material	Function	Doping [cm ⁻³]	Thickness [nm]	QD Density [/cm ² ·layer]
p-GaAs:Be	cap layer	4×10^{17}	10	
p-Al _{0.16} Ga _{0.84} As:Be	carrier confinement	4×10^{17}	25	
i-GaAs	barrier	undoped	25	
i-InAs QDs	Active region	undoped	5	1×10^{10}
i-GaAs	barrier	undoped	25	
i-InAs QDs	Active region	undoped	5	1×10^{10}
i-GaAs	barrier	undoped	25	
i-InAs QDs	Active region	undoped	5	1×10^{10}
i-GaAs	barrier	undoped	25	
i-InAs QDs	Active region	undoped	5	1×10^{10}
i-GaAs	barrier	undoped	25	
i-InAs QDs	Active region	undoped	5	1×10^{10}
i-GaAs	barrier	undoped	25	
n-Al _{0.16} Ga _{0.84} As:Si	carrier confinement	1×10^{17}	25	
n-GaAs:Si	-	1×10^{17}	10	
n-Al _{0.94} Ga _{0.06} As:Si	sacrificial layer	1×10^{18}	800	
n-GaAs	substrate	1×10^{18}		

Table 2.2 Layer structures of InAs/InGaAs quantum dot samples for infrared low-threshold photonic crystal lasers (courtesy of Yoshie)

In Tables 2.1 and 2.2, the p, i, and n in front of the material indicates the doping type: p-

Material	Layer Name	Target Thickness @ Center (nm)	Type	Target Concentration @ Center (cm ⁻³)
InGaP	Cap	10	N	2E17
{Al(x)Ga}InP	Clad	58	N	2E17
{Al(x)Ga}InP	Barrier	10	u.d.	-
InGa(x)P	2x Well	7	u.d.	-
{Al(x)Ga}InP	2x Barrier	10	u.d.	-
{Al(x)Ga}InP	Clad	58	N	2E17
InGaP		10	N	2E17
Al(x)GaAs		700	u.d.	-
GaAs	Buffer	100	u.d.	-
GaAs	Substrate		Si	

Table 2.3 Layer structures of InGaP/InGaAlP quantum well samples for visible photonic crystal lasers and submicron disk lasers

type, intrinsic, and n-type. Normally, we use Zn for the p-type, and Si for the n-type doping. For the optically pumped lasers, it doesn't necessary to put doping. However, the doping wafer would expect to have high carrier density. A cap layer is often put on top of the slab layer for protection from oxidation in case an aluminum component is present. At the end of the fabrication procedure, the cap layer would be removed by chemical wet etching, leaving the slab layer intact. The slab layer, also called the active layer, normally consists of cladding, quantum well (quantum dot), and barrier layers. Quantum well (quantum dot) layers are designed to match the wavelength range we expect. In the case of Table 2.1, the quantum wells are formed by different composition of the quaternary InGaAsP compound layer to emit light around 1550 nm. In the case of Table 2.2, the quantum dots are formed by InAs and GaAs lattice mismatch layers to emit light around 1300 nm. In the scope of

this thesis, the quantum wells are formed by a ternary InGaP compound layer and a quaternary InGaAlP compound layer to emit light around the 670 nm. Due to the different emission wavelength, the thickness of the slab layer is designed to be 330 nm, 245 nm, and 170 nm in order to contain only the fundamental mode in the vertical direction. Underneath the quantum wells, a 700 nm–1000 nm sacrificial layer was grown. This would be removed to form a two-dimensional membrane structure with large contrast in the refractive index to tightly confine in the vertical direction. The thickness of this layer prevented the leakage of the light into the substrate. The symmetric structure would ensure the high quality-factor resonator design. A buffer layer was usually applied in order to have the lattice match to the quantum well system we needed. Note that we tried to avoid doping in the quantum wells due to degradation of the quantum efficiency by the dopants. However, due to the thin cladding layer (58 nm–110 nm), the concentration of dopants in the cladding can't be very high in order to keep the quantum wells intact by diffusion during the wafer growth. In the wafer design for the electrically driven photonic crystal laser, the doping would be very crucial. The metal contact put on the device would require high doping concentration for the formation of the ohmic contacts. On the other hand, the thin cladding layer would make it very difficult to prevent metal diffusion into the quantum wells, especially when high annealing temperature and long annealing time are required to form the ohmic contact. To solve this problem, we came up with the design shown in Table 2.4.

In this design, we put 200 nm GaAs lattice matched cap layer on top of InGaP cap layer for the purpose of the contact. Since the doping for n-type is still lower than that in p-type in this material system, we still put the p-type on top and the n-type on the bottom of the slab

layer. In this way, the carriers in the devices were limited by the p-type area most. The gradient doping concentration was applied here with higher concentration away from the

Material	Function	Target Thickness @ Center (nm)	Type	Target Concentration @ Center (cm ⁻³)
GaAs	Cap	200	P	5E19 (for contact)
InGaP	Cap	10	P	8E17
{Al(x)Ga}InP	Clad	58	P	-
{Al(x)Ga}InP	Barrier	10	u.d.	-
InGa(x)P	2x Well	7	u.d.	-
{Al(x)Ga}InP	2x Barrier	10	u.d.	-
{Al(x)Ga}InP	Clad	58	N	1E17
InGaP		10	N	5E17
Al(x)GaAs		700	N	1E18
GaAs	Buffer	100	N	2E18
GaAs	Substrate		N+	2E18 or higher (for contact)

Table 2.4 Layer structures of InGaP/InGaAlP quantum well samples for electrically driven visible photonic crystal lasers and submicron disk lasers

quantum wells. We also left the top cladding without doping, since the dopant we used for p-type is zinc and it has very high diffusion coefficient. This way, we created a diffusion buffer that allows the zinc diffusion for a certain amount of length. The top layer was doped with carbon which couldn't be doped high enough in the InGaP and InGaAlP layers but GaAs. This layer was designed to dope to $10^{19}/\text{cm}^3$. The contact testing with Pt/Ti showed the excellent ohmic contacts.

2.3 Fabrication procedures

In the last section, the design of epitaxial layers for wafer growth was described. In the following sections, some other typical semiconductor fabrication technologies for creating the nano-scale lasers are presented. They include oxide film formation using PECVD, photolithography and electron beam (EB) lithography, dry etching and wet etching. We use these technologies in different steps of our fabrication procedures. And for different devices, they are slightly different which we will describe in detail in the later chapters. Here I would like to give an overview of these technologies. Why do we choose these technologies and what are the important parameters we need to pay much attention when we fabricate the devices? All the steps are important for the results. However, some are repeatable and stable while others are not.

- PECVD oxide growth

PECVD oxide growth is the one which is repeatable and the properties are stable with time and in most of the chemicals. This oxide layer was used for the hard mask of the dry etching. So the requirement of this layer is first keeping the composition of the oxide the same, and second keeping the density the same. The actual components in this layer are the mixture of Si_xO_y and Si_xN_y . By keeping the same recipe, we have had no difficulty in maintaining the same quality of this hardmask layer. For the RF power, the chamber pressure was set to 22W and 900 mtorr. The flow rate of SiH_4 and N_2O gases was set to 100 and 300 sccm, respectively. This PECVD silicon oxinitride growth recipe would give a deposition rate of about 25 nm/sec. There's another option of using Spin On Glass (SOG)

as an etch mask, instead of PECVD oxide. However, due to the stress induced by the thermal process, SOG has the possibility of cracking, and the etching rate is much slower than the PECVD oxide.

- Electron beam lithography

Other than PECVD oxide growth and wafer growth, these steps are falling into two categories: pattern defining (electron beam lithography and photolithography) and pattern transferring (dry etching, which includes reactive ion etching and inductive coupled plasma etching or chemical assist ion beam etching). Due to the small feature size of our devices (e.g., 100 nm hole size), tens of nanometers of resolution in fabrication is required.

Typical lithograph methods that could satisfy this requirement are limited to electron beam lithography and industrial photolithography technology, such as deep ultraviolet lithography, which uses KrF or ArF light sources due to the shorter wavelength. Although the latter has the advantage of fast speed and mass production, but the resolution is thus far still limited by the wavelength of the light. Focus ion beam system is sometimes used for small feature device fabrication. However, due to the high-energy ion bombardment, the surface of the devices which are exposed to the ion beam would have the problem of ion damage. For the light emitter devices we are working on, this would be very risky thing to do. In this thesis work, Leica EBPG 5000 EB lithography system has been used to define the patterns in the EB resist. Compared to the conventional EB system which was converted by scanning electron microscopy, this system has the advantages of fast speed and much larger area writing. Previously, in our group, we used the converted Hitachi S-

4500 system for EB lithography. The comparison of the parameters we normally use of these two systems is shown in Table 2.5 (courtesy of Yoshie). For the limit condition, the resolution of EBPG is less than 1 nm while the Hitachi is about 1 nm.

A proper selection of the electron beam resist is very crucial to obtain the resolution inherent to the EB lithography systems. Three types of electron beam resists were used in this thesis work: 950 K molecular weight single layer PMMA resist, ZEP520 resist, and

System	Electron Gun	V_{acc}	Beam Spot	Current
1) Hitachi S-4500	Cold Field Emission	30 kV	1 nm	50 pA
2) Leica EBPG 5000	Thermal Field Emission	100 kV	30 nm	1 nA

Table 2.5 Electron beam lithography systems used in our group. V_{acc} is the acceleration voltage. (courtesy of Yoshie)

950K/495 K bilayer PMMA resists. PMMA is an abbreviation for poly-methylmethacrylate. Both PMMA and ZEP are positive resists for high-resolution lithography. Figure 2.1 and Figure 2.2 show the scanning electron micrographs of samples after EB lithography with under exposure (lower dose) and right exposure (correct dose) respectively. ZEP520 resist was electron beam written with photonic crystal pattern and developed by amyl acetate. The bilayer PMMA resist are used when a lift-off process is needed. As for the chemical resistance, although ZEP520 resist is not as good as the photoresists, it is much better than PMMA and almost all other electron beam resists. For example, etching rate of ZEP520 in CHF_3 reactive ion etching is less than 5 nm/minute while about 40nm / minute for 950K PMMA. Hence, the selectivity of ZEP over SiON is

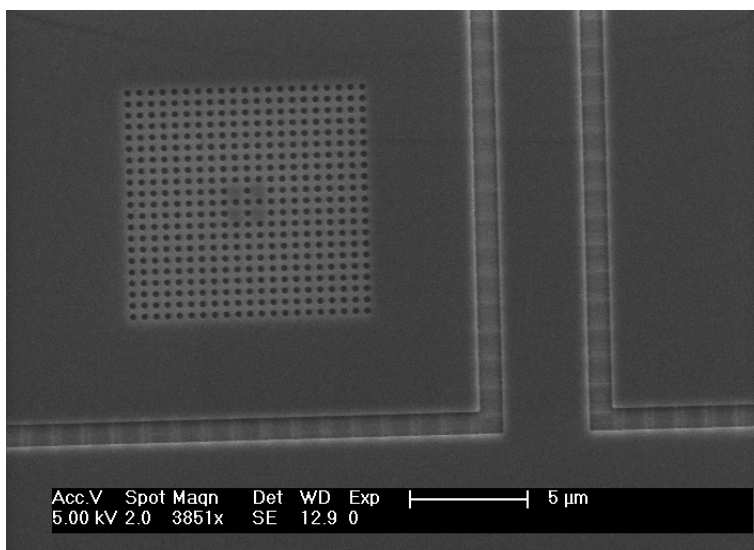


Figure 2.1 This top-view SEM micrograph shows the developed ZEP profile after EBPG electron beam writing with low beam dose. The underexposed condition could be clearly seen from the strips in the 1 micron trench area.

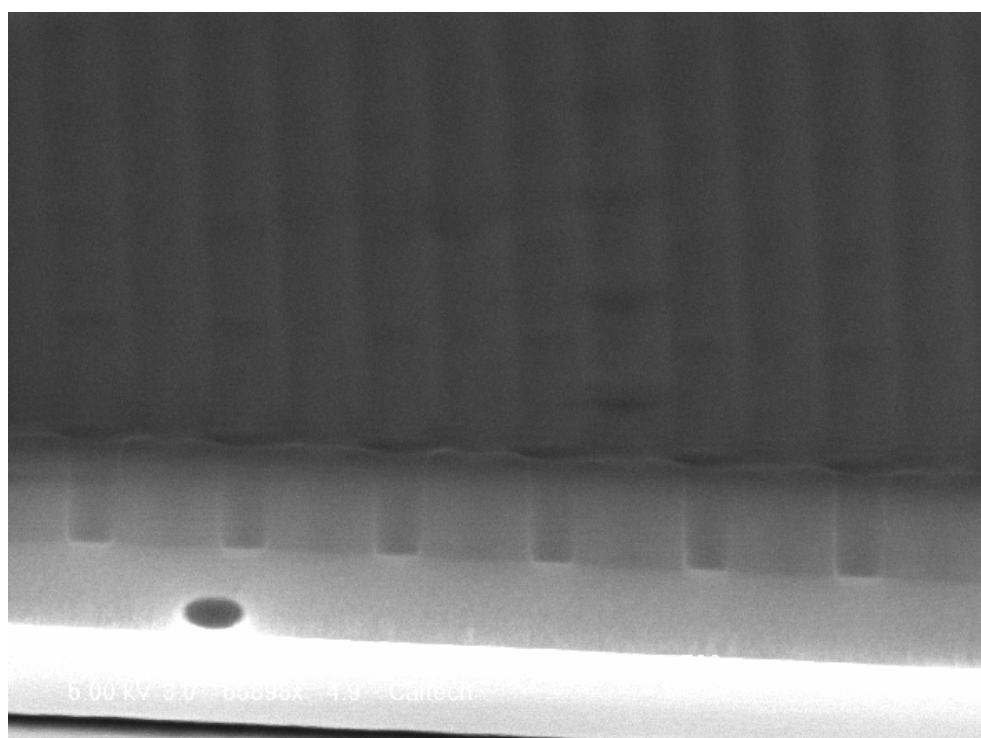


Figure 2.2 Developed ZEP profile after EBPG electron beam writing with correct dose. The hole profiles in the ZEP layer are very good. The black circle is a bubble in the SOG layer. The substrate in this photo is GaAs based InGaP/InGaAlP quantum well system. This sample was cleaved in order to show the cross-section features.

much less than PMMA over SiON (which is about 1:1 in this chemistry). This good selectivity gives us more chance to get good pattern transferring from the resist into the hardmask SiON layer. On the other hand, good chemical resistance causes problems when the resist needs to be removed. Fortunately, like many other polymers, ZEP520 decomposes when irradiated by deep ultraviolet light. In practice, a 254 nm ultraviolet light was used to irradiate the samples for about half an hour. Then 90°C hot n-methylpyrrolidone (NMP) was used to dissolve the decomposed ZEP520 resist.

- Reactive ion etching of SiON hardmask

After the EB lithography, the defined patterns were transferred into the hard etch mask layer or the substrates using the dry etching techniques. Since the quantum well layers would be exposed to the etching environment, the etching methods are required to do less damage to these layers besides the precise transferring of the pattern into the dielectric materials, such as InGaAsP or InGaP/InGaAlP. Here, four types of etching are present, depending on the material we etch.

For etching SiON hardmask, we used reactive ion etching (RIE). Compared to the barrel etcher, the RIE employs capacitively coupled plasma and provides good directional etching or anisotropic etching. Trifluoromethane (CHF_3) chemistry was used to etch the SiON layer and ZEP520 was used as an etching mask due to the good selectivity over the SiON in CHF_3 chemistry as mentioned above. The good result was obtained in our system when using 20 sccm flow rate of CHF_3 , 16 mTorr of chamber pressure, 90 W of RF power, and 3 inches parallel plate distance. The DC bias was typically around 500 V and the

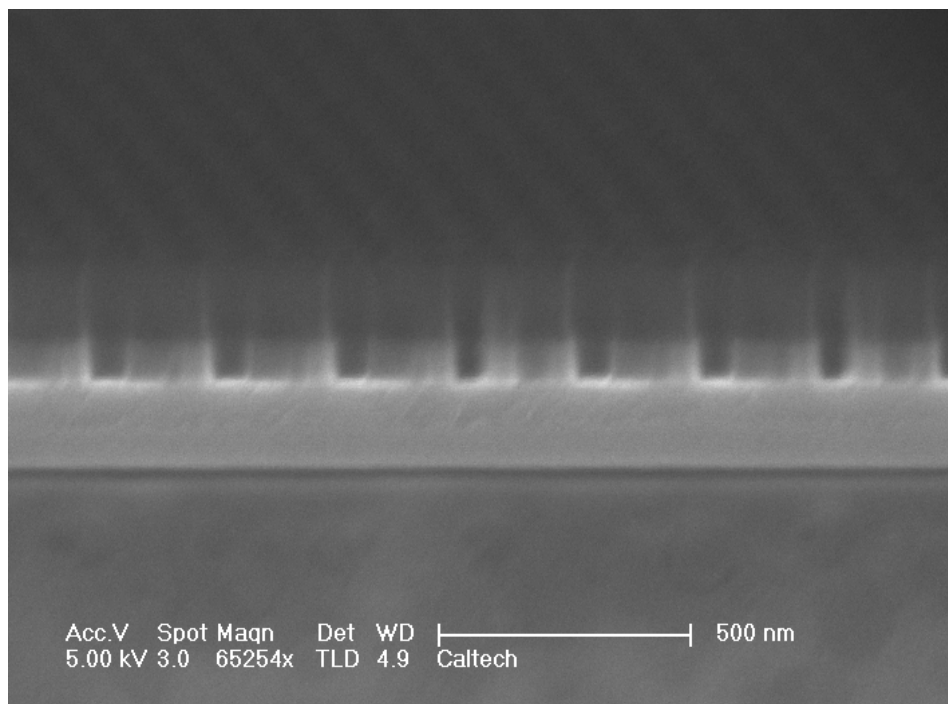


Figure 2.3 SEM micrographs of a reactive ion etching result. The CHF_3 plasma transfers the patterns in ZEP520 into the SiON etch mask. Note that the hole size in the picture is less than 100 nm.

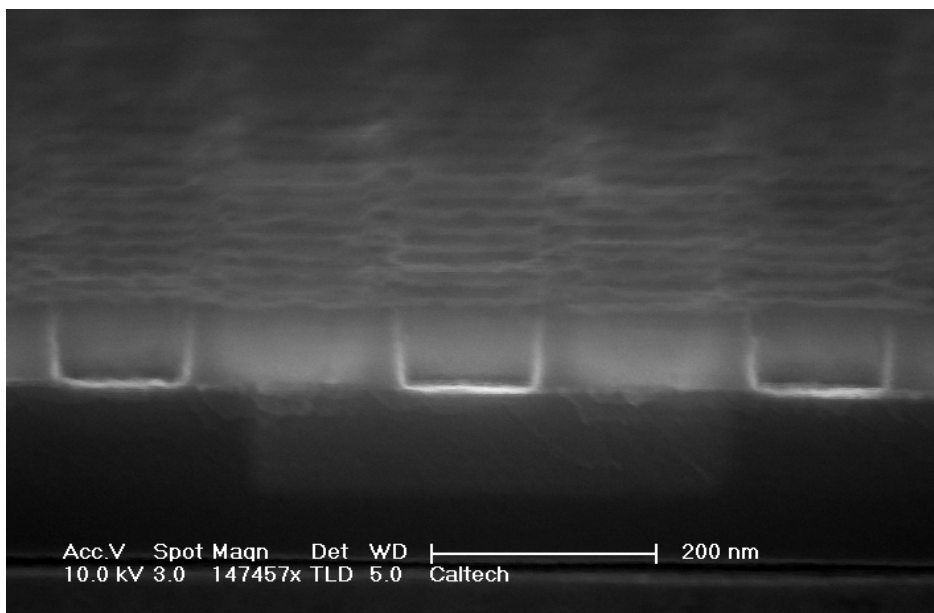


Figure 2.4 SEM image of the cross section of a ZEP removed sample with photonic crystal pattern in the 100 nm thick SiON. The roughness on the top surface may be the leftover ZEP resist which we removed using the descum in ICP.

etching rate was around 40nm/minute. Figure 2.3 shows an SEM image of a cleaved sample cross section after the CHF_3 RIE etching. After etching, the ZEP resist was removed by 254 nm deep UV exposure followed by chemical dissolution in order to have a clean etched mask for the next inductively coupled plasma (ICP) etch. Figure 3.4 shows the SEM image of the same chip after the removal of the resist.

- Inductively coupled plasma relative ion etching (ICPRIE)

The inductively driven source at 13.56MHz provides good discharge efficiency because only a small part of the voltage is dropped across the plasma sheath, which is a thin positively charged layer, and the loss of ion energy is much smaller than in capacitive coupling. Compared to RIE process, the ICPRIE has the freedom to control the plasma density and ion energy separately. Thus, the control of physical ion bombardment and chemical reaction could be more independent. Therefore, ICP-RIE etch technique could produce high aspect ratio structure without large damage to the surface of the materials.

We used hydrogen iodine (HI) and chlorine mixture for our ICP RIE etching of InGaAsP and InGaP/ InGaAlP systems. HI has the advantage of smooth etching surface and it reacts with the indium component at room temperature, while chlorine chemistry leaves InCl_3 reaction product which can only be removed at 150°C or higher temperatures. On the other hand, chlorine is a very active gas for etching the GaAs materials. The mixture of these two gases was optimized to have a better etching result for different materials. Figure 2.5 shows the InGaAsP etching result under the condition of 20 sccm, 9 sccm, 5 sccm of HI, H_2 Cl_2 flowrates respectively, 10 mTorr chamber pressure, 850 W of ICP power, and 100 W of RF

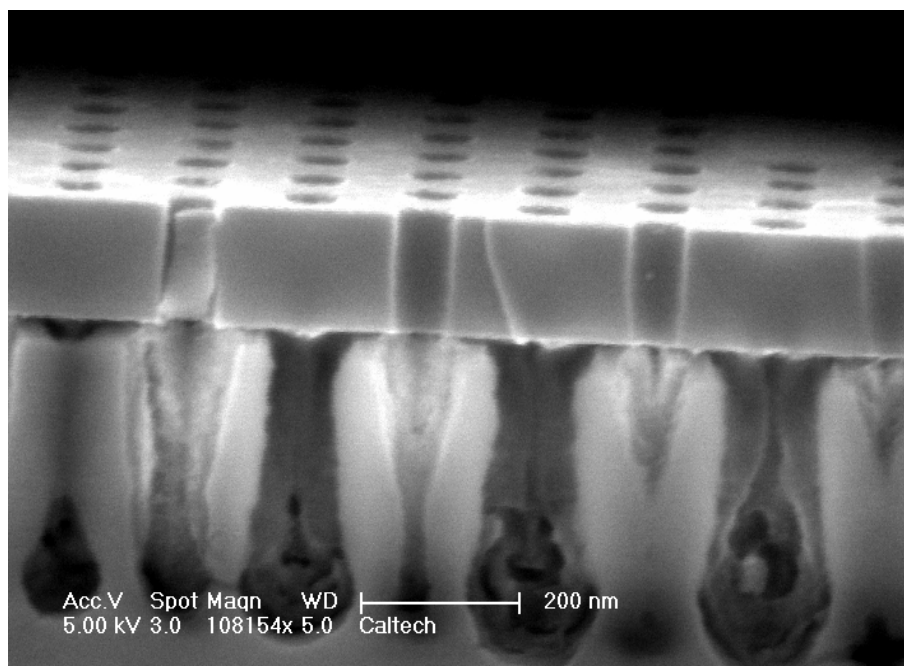


Figure 2.5 The hole profiles on the QW layer after ICP-RIE. The SiON and ZEP layers are removed. The black and white irregular shape area underneath the slab layer is due to the oxidation of AlGaAs in the air.

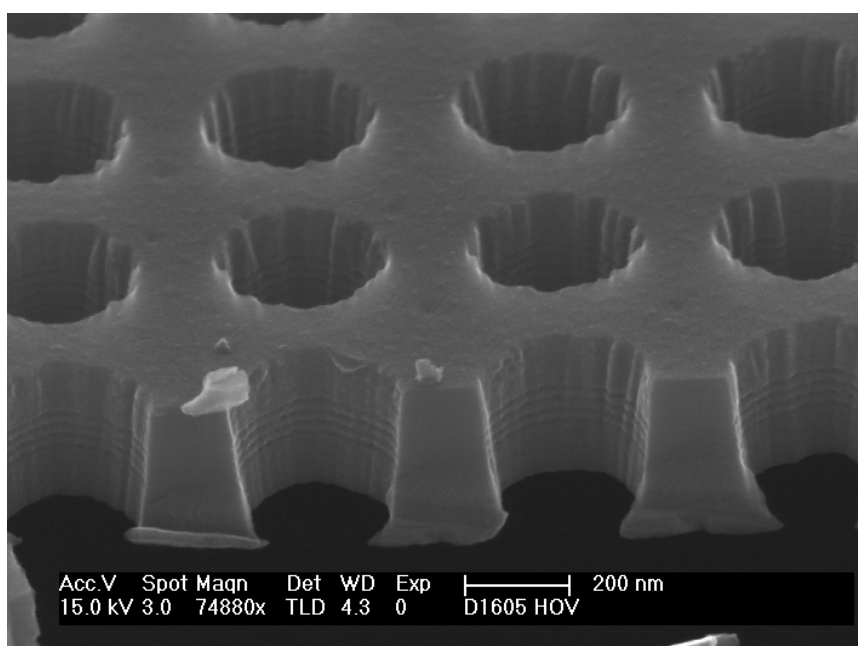


Figure 2.6 The hole profiles on the InGaAsP QW layer after ICP-RIE and chemical undercut. The inclined the sidewall was due to the short time etching of the sample. And on the image, the quantum wells are clearly seen due to the slightly chemical etching.

power. Figure 2.6 shows the InGaP/ InGaAlP etching result under the condition of 20 sccm, 10 sccm, 7 sccm of HI, H₂ Cl₂ flowrates respectively, 10 mTorr chamber pressure, 300 W of ICP power, and 100 W of RF power.

- Undercut and drying process

After the ICP RIE etching, samples were undercut and the SiON mask layers were removed using buffered hydrofluoric acid (HF). For the InGaAsP material system, the InP sacrificial layer was partially removed by diluted hydrochloric acid (HCl). For InGaP/InGaAlP material system, normally we thermal oxidized the AlGaAs sacrificial layer and then Al_xO_y was removed by potassium hydroxide (KOH). The exposure time to the air between the ICP-RIE etching and thermal oxidation is very crucial, due to the easy oxidation in the air (with water vapor in presence) of our AlGaAs sacrificial layer which has Al of 95% in the composition. The sample drying process in the end is also very important in forming symmetric slab (membrane) structures. Trapped liquid underneath the membranes pulls it down during the evaporation process due to the surface tension. This would result in bent membranes or even broken structures. In our process, we typically apply hexane or isopropyl alcohol as the last rinsing solvent because of their low surface tension. A safer way to prevent the bending of the membrane is critical point drying, in which the solvent is replaced by carbon dioxide (CO₂) liquid, due to the low critical point of CO₂. And then the temperature and pressure are increased until the solution is supercritical and the liquid changes to gas without damaging the sample.

- Photolithography and lift off

Photolithography here was used for defining the metal contact patterns for electrically pumped devices and it doesn't require as high resolution as electron beam lithography. However, sometimes, the bilayer photoresist, such as Shipley SH1812 and Shipley LOR were used together to get good lift off results.

2.4 Measurement setups

In this section, we will briefly describe the measurement setups for the laser characterization for our nano-scale lasers. All of them are micro photoluminescent setup. First is a horizontal configuration, which is better for reconstruction and good for adjusting the focal length (Figure 2.7). The second one is a vertical configuration, which is good for measuring signals from the samples in solution; also it has the advantage of easy mounting of the sample by simply placing the chip onto the stage (Figure 2.8). The third setup is for the measurement of the electrically driven devices (Figure 2.9), which incorporates the probe stations as well as the semiconductor parameter analyzer for measuring the relation between the driving current of the devices and voltage across them. Since this setup was directly built up from a vertical stereo microscope system, the magnification can be changed (rotating the objectives) without adjusting the sample's working distance. The first and the second setups are typical optical micro-photoluminescent measurement setup while the third is built to meet the need to measure electrical properties with optical properties simultaneously in the micro, nano-scale devices.

Optical Measurement

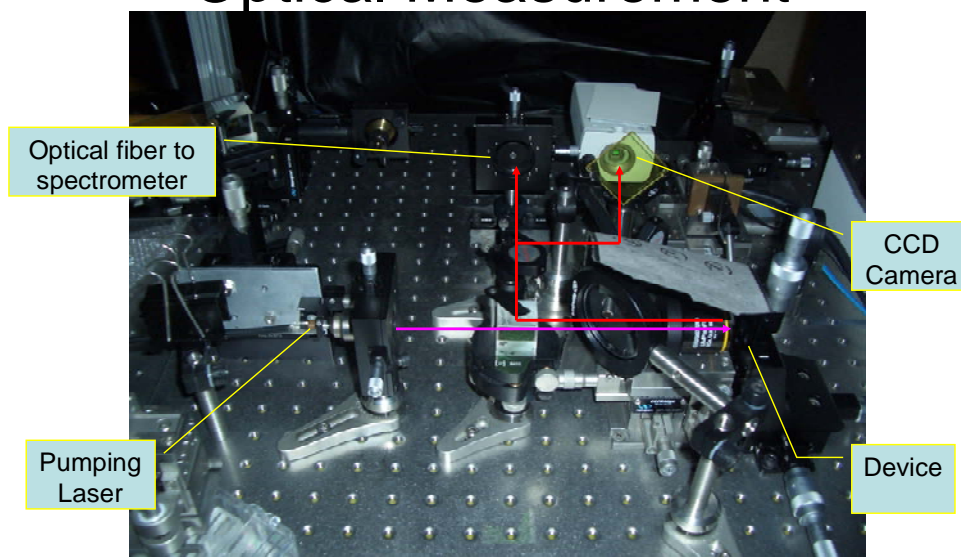


Figure 2.7. Horizontal setup for optical pumping of nanolasers. The pumping diode laser path is shown in thick line. It passes through an objective. Emissions from the sample are sent back through the same objective and through a beam splitter. The thin line path shows two possible destinations, the CCD camera to help align the sample, and the optical fiber coupled to the spectrometer.



Figure 2.8. Vertical setup for optical pumping of nanolasers. It is similar to the horizontal setup but the pumping diode laser is on top and the sample stage is placed on the optical table on the bottom. The pump light also passes through a microscope objective. Emissions from the sample are sent back through the same objective and through a splitting prism. The CCD camera is to help alignment of the sample, and the optical fiber is coupled to the spectrometer

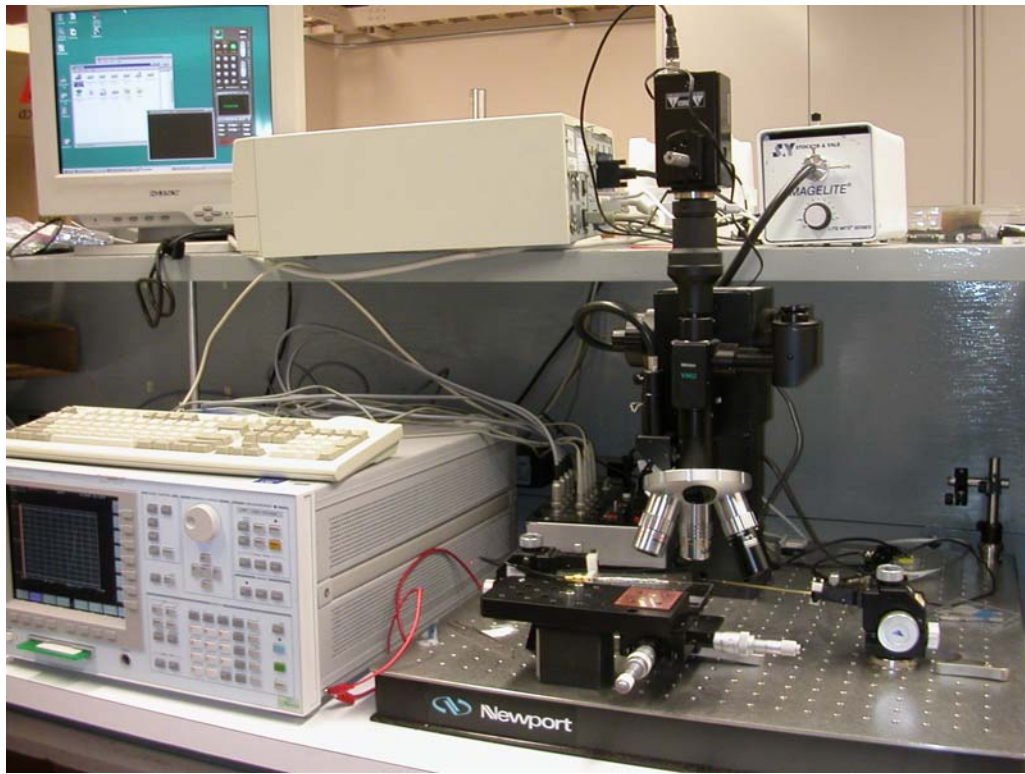


Figure 2.9. Vertical setup for electrical pump of nanolasers. The semiconductor parameter analyzer is used to characterize the metal contact as well as the device diode property. In the meanwhile, it pumps the device. The emission was collected by a stereo microscope with CCD. Three different magnification objectives enable the device alignment. The optical fiber is coupled to the cooled CCD spectrometer.